Winter 2-2-2022

Synergistic enhancement of formic acid electro-oxidation on PtxCuy co-electrodeposited binary catalysts

Yaser M. Asal
The British University in Egypt

Ahmad M. Mohammad
Cairo University

Sayed S. Abd El Rehim

Islam M. Al-Akraa
The British University in Egypt

Journal of Saudi Chemical Society (2022) **26**, 101437

King Saud University

Journal of Saudi Chemical Society

www.ksu.edu.sa
www.sciencedirect.com

ORIGINAL ARTICLE

Synergistic enhancement of formic acid electro-oxidation on Pt_xCu_y co-electrodeposited binary catalysts

Yaser M. Asal [a], Ahmad M. Mohammad [b], Sayed S. Abd El Rehim [c], Islam M. Al-Akraa [a,*]

[a] *Department of Chemical Engineering, Faculty of Engineering, The British University in Egypt, Cairo 11837, Egypt*
[b] *Chemistry Department, Faculty of Science, Cairo University, Cairo 12613, Egypt*
[c] *Chemistry Department, Faculty of Science, Ain Shams University, 11566 Abbassia, Cairo Egypt*

Received 4 December 2021; revised 16 January 2022; accepted 25 January 2022
Available online 2 February 2022

KEYWORDS

co-electrodeposition;
Fuel cells;
Pt-Cu;
Catalyst poisoning;
Formic acid

Abstract A propitious binary catalyst composed of Pt and Cu which were electrodeposited simultaneously onto a glassy carbon (GC) substrate was recommended for the formic acid (FA) electro-oxidation reaction (FAOR); the principal anodic reaction in the direct FA fuel cells (DFAFCs). The simultaneous co-electrodeposition of Pt and Cu in the catalyst provided an opportunity to tune the geometric functionality of the catalyst to resist the adsorption of poisoning CO at the Pt surface that represented the major impediment for DFAFCs marketing. The catalytic activity of the catalyst toward FAOR was significantly influenced by the (Pt^{4+}/Cu^{2+}) molar ratio of the electrolyte during electrodeposition, which also affected the surface coverage of Pt and Cu in the catalyst. Interestingly, with a molar (Pt^{4+}/Cu^{2+}) ratio of (1:4), the catalyst sustained superior (3.58 compared to 0.65 obtained at the pristine Pt/GC catalyst) activity for FAOR, concurrently with up to four-times (0.73 compared to 0.18 obtained at the pristine Pt/GC catalyst) improvement in the catalytic tolerance against CO poisoning. This associated, surprisingly, a negative shift of ca. 336 mV in the onset potential of FAOR, in an indication for the competitiveness of the catalyst to minimize superfluous polarizations in DFAFCs. Furthermore, it offered a better (ended up with 20% loss in the activity) stability for continuous (1 h) electrolysis than pristine Pt/GC catalyst (the

* Corresponding author at: The British University in Egypt (BUE), El Sherouk City, Cairo-Suez Desert Road, Cairo, Postal No. 11837, Egypt.
E-mail addresses: yasser.mohamed@bue.edu.eg (Y.M. Asal), ammohammad@cu.edu.eg (A.M. Mohammad), islam.ahmed@bue.edu.eg (I.M. Al-Akraa).

Peer review under responsibility of King Saud University.

Production and hosting by Elsevier

https://doi.org/10.1016/j.jscs.2022.101437

loss reached 35%). The impedance and CO stripping measurements together excluded the electronic element but confirmed the geometrical influence in the catalytic enhancement.

1. Introduction

According to statistics reported by International Energy Agency (IEA) and the American Energy Information Administration (EIA), the global energy consumption increases by 50 quadrillion Btu every year [1]. From another perspective, the intensive dependence on fossil fuels for electricity generation has absolutely altered our ecosystem [2–8]. Hence, research has been oriented to offer clean, abundant, and renewable sources for energy that suffice the global consumption and maintain a safe environment.

In this context, fuel cells (FCs) appeared promising as advanced electrochemical energy converters of featured environmental flexibility, and high efficiency at low operating temperatures [9–12]. Technically, FCs convert directly and efficiently (up to 60%) the chemical energy into electricity with a tremendous (up to 90%) reduction in major pollutants [13]. The polymer electrolyte membrane FCs (PEMFCs) that belongs to the low-temperature FCs that utilize solid polymeric electrolyte for the ionic conduction has attracted a special attention due to their robustness, high power density, and low operational temperature. Of these low-temperature PEMFCs, the direct methanol FCs (DMFCs) and hydrogen FCs (HFCs) offered, recently, a comprehensive interest for electric vehicles and portable electronics [6,14,15]. However, their fast commercialization has been restricted by the huge cost of H_2 containers, the prospective risks during H_2 transportation and the toxicity and crossover of methanol [2,5,16]. Hence, the DFAFCs appeared more attractive owing to their higher theoretical open circuit potential (1.45 V compared to 1.23 V of HFCs and 1.21 V of DMFCs), lower toxicity, non-flammability and lower crossover through the Nafion membrane [17–20].

Till now, the most common anodic catalysts for DFAFCs are mainly based on noble Pt and Pd metals [11,21–24]. However, Pt revealed a higher stability than Pd due to its higher dissolution resistance in harsh reaction conditions [25,26]. However, unfortunately, Pt can easily be poisoned by some reaction intermediates, such as carbon monoxide (CO) [27–29]. Several investigations reported that FAOR proceeds at Pt surfaces with a double-pathway mechanism [2,16,30–33]. The direct pathway which involves the direct oxidation of FA to CO_2 (Eq. (1)) and the indirect pathway which involves the non-*faradaic* adsorption of poisoning CO at the Pt surface (Eq. (2)) followed by its subsequent oxidation at a high overvoltage (Eq. (3)).

o Direct dehydrogenation pathway:

$$HCOOH \rightarrow CO_2 + 2H^+ + 2e^- \quad (1)$$

o Indirect dehydration pathway:

$$HCOOH \rightarrow CO_{ads} + H_2O \quad (2)$$

$$CO_{ads} + H_2O \rightarrow CO_2 + 2H^+ + 2e^- \quad (3)$$

Considering the huge cost of Pt catalysts, it became crucial to amend it with a cheaper modifier to increase its utilization efficiency and catalytic performance [34,35]. In fact, previous modifications of Pt with metals (e.g. Au [32], Pd [36], Bi [37] and/or metal oxides (e.g., oxides of Ni [30], Mn [2], Cu [38], and Fe [39])) could greatly sustain better performance toward FAOR with enhanced structural and/or electronic properties.

Although the difficultness in controlling size, shape and distribution of the catalyst component [20], electrodeposition represents a facile, fast and economic technique for assembling metal and metal oxide modified catalysts; ensuring a controlled production of a smooth surface with strong bonding with the substrate and offering opportunities for alloys and composite coatings with high hardness [40].

In this study, a binary catalyst composed of Pt and Cu was fabricated onto the GC (a typical substrate for the deposition of nanoparticles that can be used for a simple investigation) and proved competent for FAOR. The catalyst was synthesized by the "simultaneous co-electrodeposition" protocol that ensured a convenient homogeneity of the catalytic constituents that were added in minute loadings (relatively to other procedures as the layer-by-layer approach) [2,32]. The molar Pt^{4+}/Cu^{2+} ratio of the electrolyte during the catalyst's deposition was optimized to attain the highest catalytic activity toward FAOR. Furthermore, the catalyst's morphology, surface composition, and molecular structure were inspected to address the remarkable enhancement of these catalysts toward FAOR.

2. Experimental

2.1. Chemicals and electrodes

Copper (II) sulfate pentahydrate ($CuSO_4{\cdot}5H_2O$, 99%), sodium hydroxide-pellets (NaOH), sodium sulfate anhydrous (Na_2SO_4), and FA (HCOOH, 98%) were purchased from Alfa Aesar while dihydrogen hexachloroplatinate (IV) hydrate (Premion®, $H_2PtCl_6{\cdot}6H_2O$, 99.9%, metals basis) and sulfuric acid (AR, H_2SO_4, 98%) were purchased from Sigma Aldrich. All chemicals were of high purity and were used as received without further purification. A three-electrode electrochemical cell was used for the catalyst's preparation and electrochemical and catalytic inspections. A cleaned (by mechanical polishing with aqueous slurries of successively finer alumina powder (down to 0.06 mm) followed by a thorough washing with second distilled water) pristine and modified glassy carbon (GC) electrode (5.0 mm diameter) of a geometric area of ca.

0.196 cm^2 was used as the working electrode, a spiral Pt wire was used as the counter electrode and an Ag/AgCl/NaCl (3 M) electrode was used as the reference electrode. All potentials were measured relative to this Ag/AgCl/NaCl (3 M) reference electrode.

2.2. Catalyst preparation

The "simultaneous co-electrodeposition" technique was employed to prepare Pt_xCu_y catalysts onto the GC electrode surface with several molar ratios (starting from 1:0 till 1:4) [2,32]. The electrolyte of electrodeposition was 0.1 M Na_2SO_4 aqueous solution containing 2.0 mM $H_2PtCl_6{\cdot}6H_2O$ and 2.0 mM $CuSO_4{\cdot}5H_2O$ For all catalysts, the electrodeposition of Pt and Cu onto the GC electrode surface was carried out potentiostatically at −0.2 V permitting the passage of only 9.4 mC.

For a simple recognition of the electrodes' preparation, an abbreviation of Pt_xCu_y was assigned to recognize the molar ratio of Pt^{4+} to Cu^{2+} in the deposition electrolyte, where x and y referred to the molar ratios of Pt^{4+} and Cu^{2+} ions, respectively. For example, the catalyst denoted as Pt_1Cu_4 correspond to a mole ratio of 1:4 for Pt^{4+} to Cu^{2+} ions in the deposition electrolyte.

2.3. Electrochemical measurements

All electrochemical experiments were tested at room temperature (ca. 25 ± 1 °C) in aqueous solutions using a Bio-Logic SAS Potentiostat (model SP-150) operated with EC-Lab software. The electrocatalytic performance of the Pt_xCu_y catalysts toward FAOR was inspected in aqueous solutions containing 0.3 M FA (pH ~3.5). The pH was adjusted by a dilute solution of NaOH. Current densities were always calculated on the basis of real Pt surface areas of the working electrodes (as Fig. S1 shows) employing a reference value of 420 μC cm^{-2} [41].

2.4. Characterizations

The morphology and elemental composition of Pt_xCu_y catalysts were evaluated using a field-emission scanning electron microscope (FE-SEM, Quattro S, Thermo Fisher Scientific USA) whose accelerating voltage extended from 200 V to 30 kV with a magnification range from 6 to 2500000x that equipped with an energy dispersive X-ray spectrometer (EDS, AMETEK USA Element Detector). The crystallographic information of Pt_xCu_y catalysts was obtained using a high resolution X-ray diffractometer (XRD-PANalytical X'Pert Pro powder) that operated with a Cu anode, wavelength 0.154 nm, maximum 2.2 kW, and 60 kV. The inductively coupled plasma mass spectrometry, ICP-MS, (8800 ICP-MS, Agilent Technologies) was employed to assess the dissolution (loss) of Pt and Cu from the catalysts after stability measurements.

3. Results and discussion

3.1. Electrochemical characterization

Fig. 1a (Pt_1Cu_0 catalyst) displays the characteristic performance of a poly-Pt electrode in an acidic medium. This demonstrated the oxidation of Pt which extended over a potential range between ca. 0.6 and 1.2 V and coupled with the subsequent PtO reduction at ca. 0.46 V. Furthermore, the peaks that appeared in the potential range between 0 and −0.2 V were assigned to the hydrogen adsorption/desorption ($H_{ads/des}$) at the Pt surface [25]. For Fig. 1b–e, the current intensities of the $H_{ads/des}$ and PtO reduction peaks were gradually decreased with a parallel decrease in the intensity of the PtO reduction peak. This resulted from the distribution of the deposition charge between Pt and Cu which further indicated the successful deposition of Cu. As a result of Cu deposition, a new redox couple corresponding to the Cu oxidation (at ca. 0.45 V) and its subsequent reduction (at ca. 0.25 V) was developed [42–44]. With the further increase of Cu^{2+} in the solution (Fig. 1d and 1e), the current intensities of the $H_{ads/des}$ and PtO reduction peaks continued decreasing significantly concurrently with an observable increase in the current intensity of the Cu oxidation peak which appeared split [45,46] in two peaks; at 0.05 V and 0.45 V (almost similar to those obtained at the Pt_0Cu_1 catalyst (Fig. S2A)) to infer about a possible phase transformation. The calculated Pt surface area for all proposed catalysts was additionally calculated, based on the procedures in Fig. S1, as appeared in Table S1.

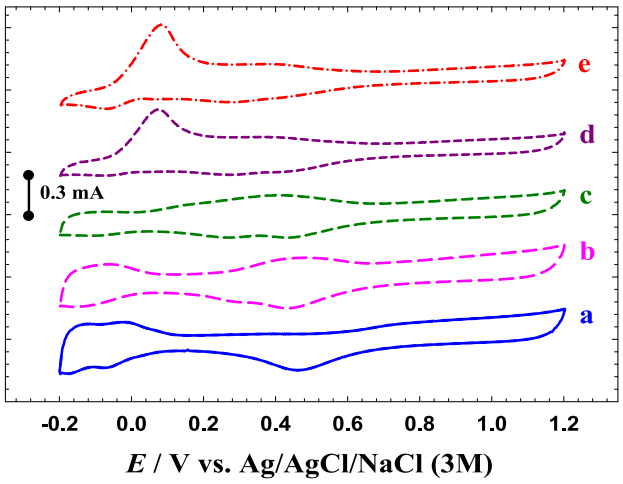

Fig. 1 CVs measured in 0.5 M H_2SO_4 at (a) Pt_1Cu_0, (b) Pt_1Cu_1, (c) Pt_1Cu_2, (d) Pt_1Cu_3, and (e) Pt_1Cu_4 catalysts. (Potential scan rate = 100 mV s^{-1}).

3.2. Morphological, compositional, and structural characterizations

The investigation is directed to elucidate the surface morphology, elemental composition, and molecular structure of the proposed Pt_xCu_y catalysts. Fig. 2 displays FE-SEM micrographs of the Pt_1Cu_0, Pt_1Cu_1, Pt_1Cu_2, Pt_1Cu_3, and Pt_1Cu_4 catalysts. As obviously seen in Fig. 2A, the deposition of Pt (Pt_1Cu_0 catalyst) occurred in spherical shape (ca. 110 nm in average diameter) with intensive aggregations (~500 nm in diameter each). This morphology was retained for Pt with the deposition of Cu in starfish and/or intersected laminar structures (almost similar to the Cu morphology for the Pt_0Cu_1 catalyst appeared in Fig. S2B) in the Pt_1Cu_1, Pt_1Cu_2, Pt_1Cu_3, and Pt_1Cu_4 catalysts (Fig. 2B-E).

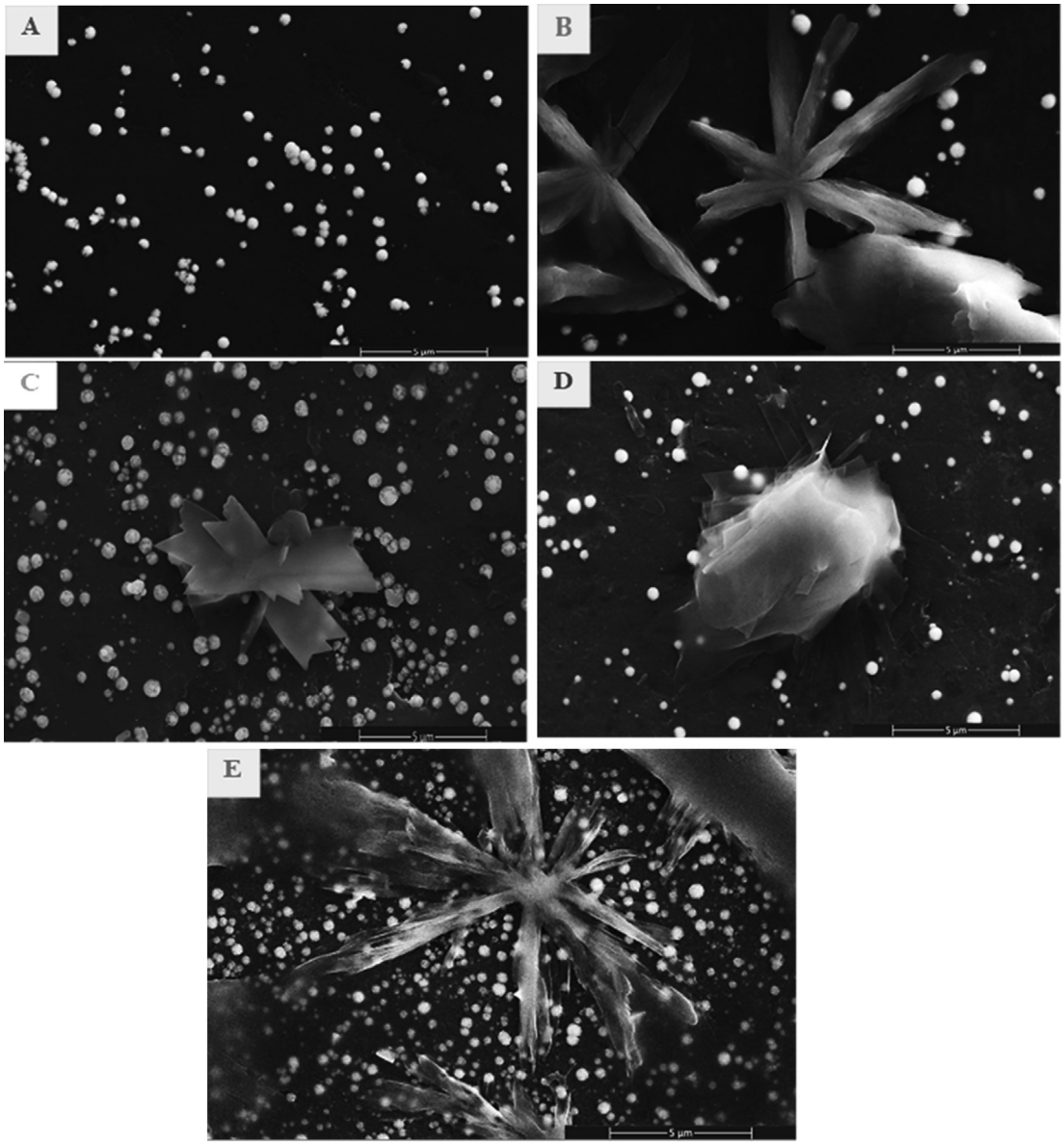

Fig. 2 FE-SEM micrographs of the (A) Pt_1Cu_0, (B) Pt_1Cu_1, (C) Pt_1Cu_2, (D) Pt_1Cu_3, and (E) Pt_1Cu_4 catalysts.

Moreover, the EDS spectra of the Pt_1Cu_0, Pt_1Cu_1, Pt_1Cu_2, Pt_1Cu_3, and Pt_1Cu_4 catalysts (Fig. 3a-e, respectively) provided a confirmation for the deposition of catalytic ingredients in the different catalysts where all peaks of C, O, Pt, and Cu appeared in their expected positions [47–49]. The elemental mapping of the Pt_1Cu_0 and Pt_1Cu_4 catalysts demonstrated the homogeneous distribution of C, O, Pt, and Cu elements in the proposed catalysts (Figs. S3A and B, respectively).

Furthermore, the crystal structures of the different Pt_xCu_y catalysts were examined by XRD (Fig. 4a-e) where several diffraction peaks were identified for all catalysts at ca. 25°, 43° and 79° corresponding, respectively, to the (002), (100), and (110) planes of the hexagonal carbon structure (JCPDS card No. 075-1621) [50]. Also, the diffraction peaks identified at ca. 38.6°, 44.6°, 65.4°, and 78.7° for all catalysts were assigned, respectively, to the (111), (200), (220), and (311) planes of the face-centered cubic (fcc) Pt lattice (JCPDS card No. 96-101-1112) [32,51]. The Pt_1Cu_1, Pt_1Cu_2, Pt_1Cu_3, and Pt_1Cu_4 catalysts showed three diffraction peaks at 2θ of ca. 43.1°, 50.2°, and 73.7°, consistent with those observed for the Pt_0Cu_1 catalyst (Fig. S2C), which were assigned to the (111), (200), and (220) facets of metallic Cu (JCPDS card No. 96-901-3016) [52–54]. The very small positive shift (ca. 0.05°) in the Pt diffractions in the Cu-modified catalysts might account for the composition change of the catalyst surface and/or Pt-Cu alloying [55].

3.3. FAOR: Activity studies

Fig. 5 (for easy comparison, all subfigures in Fig. 5 were grouped in a single figure - Fig. S4) represented the influence of Pt^{4+} and Cu^{2+} relative molar ratio in the deposition elec-

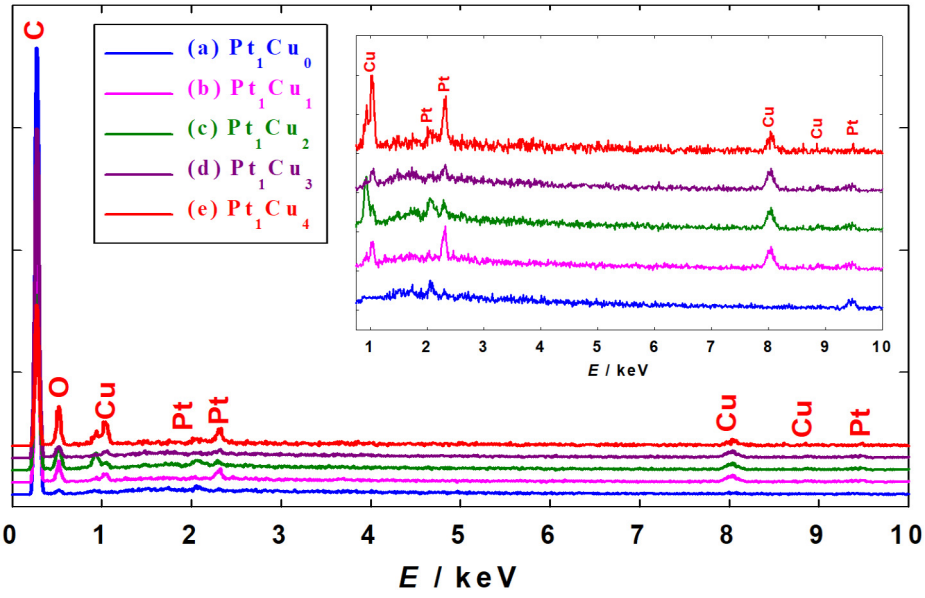

Fig. 3 EDS spectra of the (a) Pt_1Cu_0, (b) Pt_1Cu_1, (c) Pt_1Cu_2, (d) Pt_1Cu_3, and (e) Pt_1Cu_4 catalysts. The inset shows a clear view of the Pt and Cu peaks.

trolyte on the catalytic activity of the proposed Pt_xCu_y catalysts toward FAOR. First, it worth to point the inactivity of the unmodified GC electrode [56] and Cu [57] toward FAOR (see Fig. S2D). A blank test was carried out in FA-free solution (FAFS) that has the same pH (3.5) with the same measuring conditions to confirm our interpretation (will be mentioned later in text) for the peaks associated with FAOR. Fig. S5 confirmed that in FAFS, no peaks were detected at the same potentials like in case of the solution contacting FA. In Fig. 5A (Pt_1Cu_0 catalyst), two oxidation peaks were observed in the forward (anodic-going) scan at 0.34 V and 0.8 V. The first peak (at ca. 0.34 V) was assigned to the direct (preferred, because of its lower anodic overpotential that turns the output voltage of DFAFCs higher) oxidation of FA to CO_2 (Eq. (1)). The current density of this peak will be abbreviated as I_p^d. The second peak (ca. 0.8 V) was assigned to the oxidation of the CO_{ads} to CO_2 (Eq. (3)) after the hydroxylation of the Pt surface at a potential of ca. 0.7 V. The current density of this peak will be abbreviated as I_p^{ind} [58]. In reality, the core challenge of assigning Pt-based catalyst for FAOR is related to the adsorption of CO (CO_{ads}) which occurs spontaneously from the non-*faradaic* dissociation of FA at open circuit potentials (Eq. (2)). This deactivates the Pt surface and prompts a potential poisoning for a significant number of Pt active sites, which, in turns, impede the direct "preferred" pathway of FAOR. Balandin proposed the "Multiplet theory" that investigated the simultaneous adsorption of reacting species to a group of active atoms of a given catalyst [59]. He proposed a correspondence between the geometry of active centers and the energies of forming and breaking chemical bonds of the adsorbate/adsorbent clusters. According to this theory, the adsorption of CO on the Pt surface requires the presence of three neighboring Pt active sites with a certain geometry. If this contiguity was disturbed, the Pt–CO bonding will not form; as will be elaborated below. In the backward (cathodic-going) scan, the Pt surface became clean (free of poisoning CO_{ads}) after the oxidation of poisoning CO_{ads} and that boosted FAOR as shown from the high peak current density of the backward scan (I_p^b).

For the Pt_1Cu_1, Pt_1Cu_2, Pt_1Cu_3, and Pt_1Cu_4 catalysts, critical changes appeared and influenced the relative ratios of I_p^d, I_p^{ind}, and I_p^b which denote important catalytic information. Generally, the I_p^d/I_p^{ind} ratio evaluates the enhancement in the catalytic activity in the favorable direct oxidation pathway. On the other hand, the I_p^d/I_p^b ratio estimates the catalytic tolerance of the catalyst for poisoning CO species. These changes in current densities can associate a further change in the onset potential of the direct FAOR, E_{onset} (measured at a constant current density of ca. 0.2 mA cm^{-2}), that reflects the capability of the catalyst to overcome unnecessary overpotentials (particularly of charge transfer) that normally detracts the voltage output of the cell. The I_p^d/I_p^{ind} ratio of the Pt_1Cu_0 catalyst

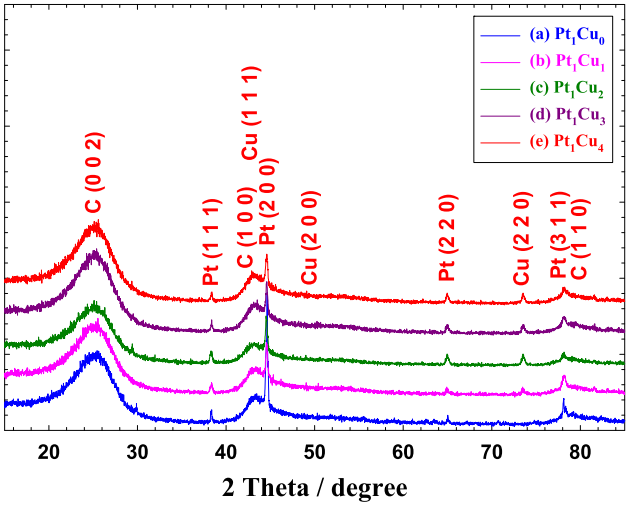

Fig. 4 XRD pattern of the (a) Pt_1Cu_0, (b) Pt_1Cu_1, (c) Pt_1Cu_2, (d) Pt_1Cu_3, and (e) Pt_1Cu_4 catalysts.

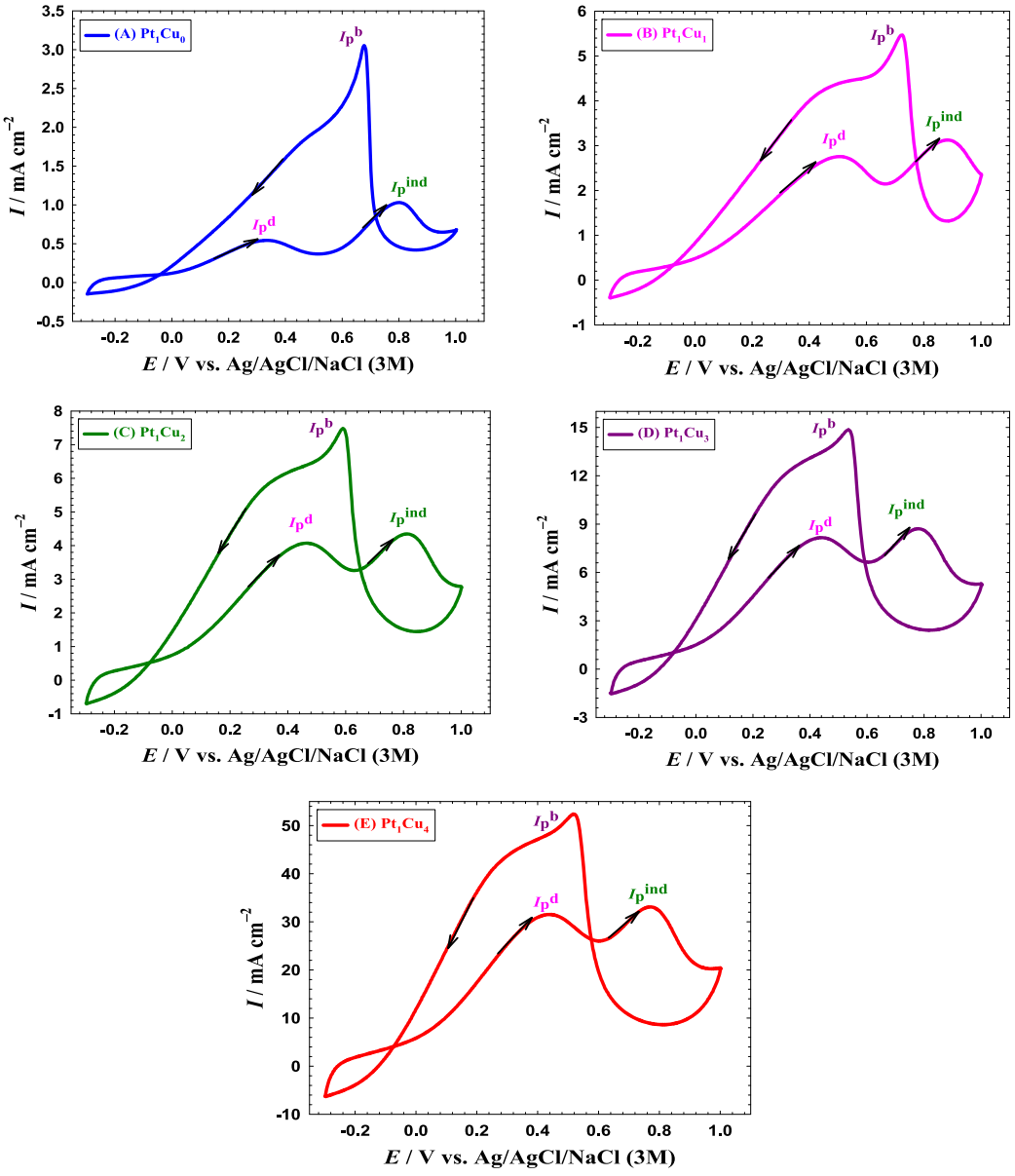

Fig. 5 CVs for FAOR (potential scan rate = 100 mV s^{-1}) at (A) Pt_1Cu_0, (B) Pt_1Cu_1, (C) Pt_1Cu_2, (D) Pt_1Cu_3, and (E) Pt_1Cu_4 catalysts in aqueous solution of 0.3 M FA (pH ~3.5).

was ca. 0.65 (see Table 1), which is low to permit the movement for DFAFCs into a real commercialization. The increase of this I_p^d/I_p^{ind} ratio of the catalyst is highly important for a commercial purpose. Fascinatingly, the CVs in Fig. 5B-E and the catalytic data in Table 1 demonstrated the importance of adding Cu to the catalysts and elaborated the influence of varying the (Pt^{4+} and Cu^{2+}) molar ratios in the deposition electrolyte on the catalytic activity toward FAOR. Interestingly, both of I_p^d/I_p^{ind} and I_p^d/I_p^b increased with the increase in the Cu^{2+} molar ratio. This reflected the critical role of Cu to direct FAOR in the direct pathway and to mitigate the CO poisoning. In addition, with the increase in Cu^{2+} molar ratio, a regular negative shift in E_{onset} was observed. The best catalytic data was obtained for the Pt_1Cu_4 catalyst whose I_p^d/I_p^{ind} was 3.58 (i.e., 6-times as that of the Pt_1Cu_0 catalyst). Its I_p^d/I_p^b was also the highest (0.73, i.e., 4-times as that (0.18) of the Pt_1Cu_0 catalyst). The negative shift in E_{onset} of this Pt_1Cu_4 catalyst was as well the largest (ca. 336 mV). Fig. 6 represents graphi-

Table 1 Electrochemical indices of the Pt_xCu_y catalysts (data were extracted from Fig. 5).

Catalyst	I_p^d/I_p^{ind}	I_p^d/I_p^b	E_{onset}/mV
Pt_1Cu_0	0.65	0.18	82.3
Pt_1Cu_1	2.44	0.61	−185.2
Pt_1Cu_2	2.89	0.65	−225.7
Pt_1Cu_3	3.11	0.67	−244.2
Pt_1Cu_4	3.58	0.73	−253.7

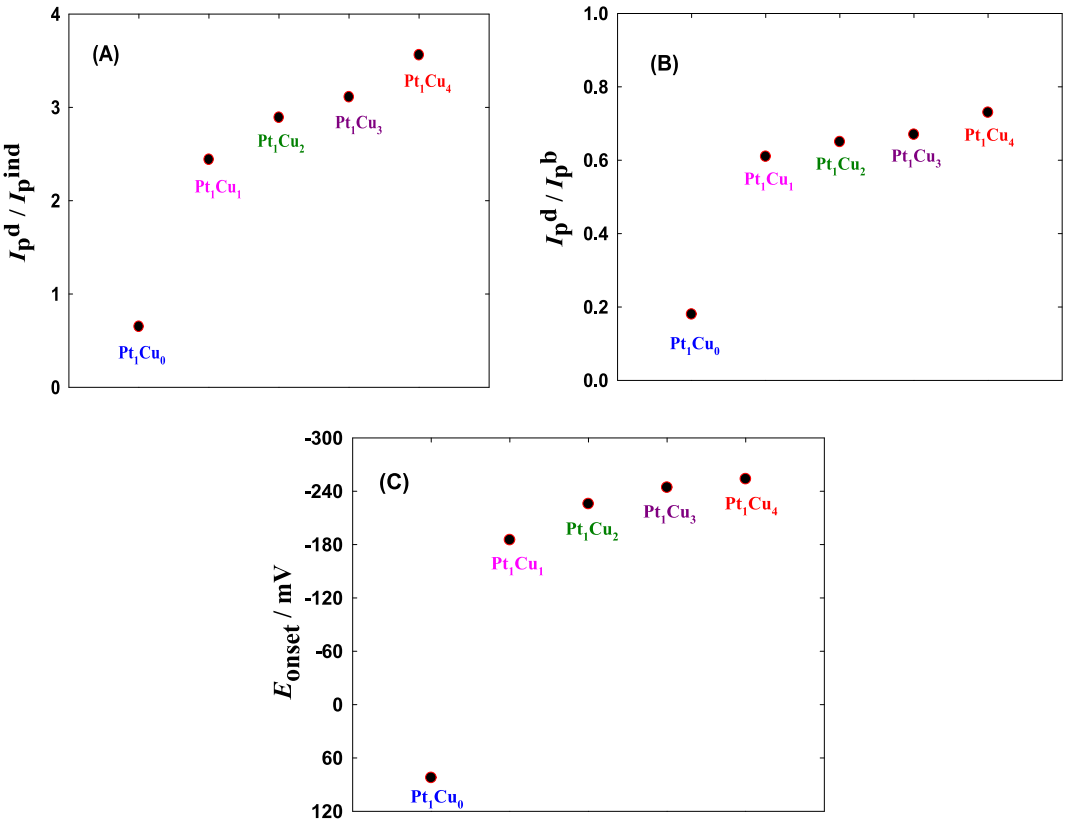

Fig. 6 The dependency of (A) I_p^d/I_p^{ind}, (B) I_p^d/I_p^b, and (C) E_{onset} on the Pt_xCu_y molar ratio.

cally these catalytic data. Also, several other parameters such as the potentials at I_p^d, I_p^{ind}, and I_p^b (E_p^d, E_p^{ind}, and E_p^b, respectively) were monitored and tabulated in Table S2. The potential changes associated with FAOR may relate to the surface composition change of the proposed catalysts.

It is important to mention that the catalytic activities of the Pt_1Cu_5 and Pt_1Cu_6 (see Figs. S6A and B and data in Table S3) catalysts toward FAOR were lower than that of the Pt_1Cu_4, presumably due to the too low loading of the active (Pt) component in the catalysts. Hence, the Pt_1Cu_4 represented the best catalyst for FAOR among all the inspected catalysts in this investigation. Interestingly, this activity surpassed many of the reported activities for FAOR in literature (see Table S4 in the supplementary data file).

3.4. FAOR: Stability monitoring

Another important measurement besides the catalyst's activity is related to the catalyst's stability. Herein, the catalyst's modification with Cu was proposed not only to promote the catalytic activity but also to enhance the stability of the catalyst, which quickly deteriorates during continuous electrolysis. The stability of the entire set of our proposed catalysts were assessed by chronoamperometric measurements (see Fig. 7) for 3600 s at a constant potential of 0.2 V. Fig. 7 (a-e, respectively) displays the current transients (*i-t* curves) of the Pt_1Cu_0, Pt_1Cu_1, Pt_1Cu_2, Pt_1Cu_3, and Pt_1Cu_4 catalysts in aqueous solution of 0.3 M FA (pH ~3.5) at 0.2 V. As obviously seen in Fig. 7a and the attached inset, the current density of the Pt_1Cu_0 catalyst decayed rapidly due to the accumulation of poisoning CO on the Pt surface. This decay diminished largely for the Pt_1Cu_1, Pt_1Cu_2, Pt_1Cu_3, and Pt_1Cu_4 catalysts (see Fig. 7b-e). Interestingly, the highest stability was also recorded for the Pt_1Cu_4 catalyst (20% loss in the catalytic activity compared to 35% for the Pt_1Cu_0 catalyst, see Fig. 7a and e). This represented an additional merit for Cu in boosting the catalytic tolerance of the Pt_xCu_y catalysts against CO poisoning during FAOR.

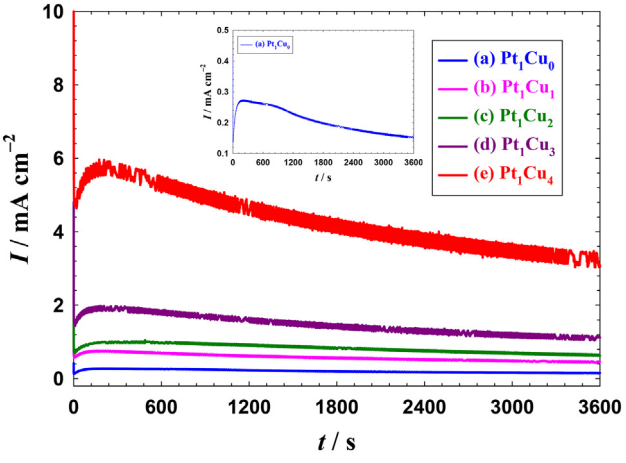

Fig. 7 Chronoamperometric curves (*i-t*) measured at (a) Pt_1Cu_0, (b) Pt_1Cu_1, (c) Pt_1Cu_2, (d) Pt_1Cu_3, and (e) Pt_1Cu_4 catalysts in aqueous solution of 0.3 M FA (pH ~3.5) at 0.2 V. The inset displays an obvious vision of the current decay of Pt_1Cu_0 catalyst.

Table 2 ICP-MS-MS data for inspected catalysts after electrochemical measurements.

Analyte	Catalyst	Conc (sample)/ μgL^{-1}
Pt	Pt_1Cu_0	1.32
	Pt_1Cu_1	0.96
	Pt_1Cu_2	0.86
	Pt_1Cu_3	0.37
	Pt_1Cu_4	0.27
Cu	Pt_1Cu_0	0.00
	Pt_1Cu_1	30.2
	Pt_1Cu_2	61.6
	Pt_1Cu_3	148.4
	Pt_1Cu_4	278.0

The ICP-MS was employed to assess the loss in the catalytic ingredients (Pt & Cu) after the electrochemical stability inspection. As expected, a loss in Cu was observed, which was expected for Cu at high potentials. This loss in Cu increased with the molar ratio of Cu^{2+} ions in the deposition electrolyte (Table 2). On contrary, the loss of the active and precious material (Pt) in the Pt_1Cu_0, Pt_1Cu_1, Pt_1Cu_2, Pt_1Cu_3, and Pt_1Cu_4 catalysts was relatively minor and got decreased with the Cu^{2+} molar ratio (Table 2). This reinforced the role of Cu in boosting the durability of the Pt_xCu_y catalysts and in ranking the Pt_1Cu_4 catalyst the best for FAOR.

3.5. FAOR: Mechanisms of enhancement

Electrochemical impedance spectroscopy (EIS) was used to interpret the catalysis of FAOR on the Pt_xCu_y catalysts. The charge transfer resistance (R_{ct}) of the proposed Pt_xCu_y catalysts was correlated to their catalytic performance toward FAOR [13,60,61]. Fig. 8 (a-e, respectively) represents the Nyquist plots for all catalysts in aqueous solution of 0.3 M FA (pH ~3.5) at a potential of 0.2 V in the frequency range between 10 mHz and 100 kHz. The data fitting was carried out using the EC-Lab software and the equivalent circuit of this system was displayed in the inset of Fig. 8. Over there, R_s and C_{dl} referred to the solution resistance and double layer capacitance, respectively, of the electrochemical system. Analysis of R_{ct} for the whole set of catalysts grouped them in two categories; one of a lower and another of a higher R_{ct} than that (0.21 kΩ) of the unmodified Pt_1Cu_0 catalyst (Fig. 8a). The Pt_1Cu_1 and Pt_1Cu_2 catalysts recorded 0.14 and 0.15 kΩ, respectively, for R_{ct} as obviously seen from their smaller semicircle diameters (Fig. 8b and c). Such a decrease in R_{ct} inferred the existence of an electronic element in the catalytic enhancement [5,13]. This electronic enhancement could possibly result from the Pt-Cu alloying that might affect the Pt–FA, Pt–CO_2 and/or Pt–CO bonding or perhaps from the participation of Cu with its higher electrical conductivity than Pt [62,63] in the reaction mechanism of FAOR in the way facilitating the kinetics of charge transfer. This might associate a structural influence that could synergistically boost the catalytic enhancement. Surprisingly, the Pt_1Cu_3 and Pt_1Cu_4 catalysts owned higher (0.27 and 0.43 kΩ, respectively) R_{ct} than that of the Pt_1Cu_0 catalyst with larger semicircle diameters (Fig. 8d and e). This came consistent with diminishing the active Pt surface and the appearance of redox pair for copper (recall the splitting of the Cu peak that appeared only in Fig. 1d and e) that probably deactivated Pt electronically toward FAOR. This electronic deactivation was not equivalent to the geometrical (structural, third body) influence that Cu added to Pt which boosted synergistically the catalytic activity of the Pt_1Cu_3 and Pt_1Cu_4 catalysts toward FAOR. Table 3 summarizes the electrochemical data (R_s and R_{ct}) obtained from Fig. 8.

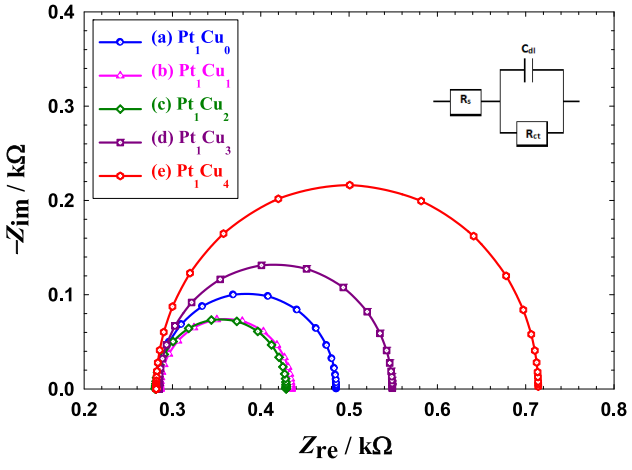

Fig. 8 Nyquist plots obtained of the (a) Pt_1Cu_0, (b) Pt_1Cu_1, (c) Pt_1Cu_2, (d) Pt_1Cu_3, and (e) Pt_1Cu_4 in aqueous solution of 0.3 M FA (pH ~3.5). The AC potential amplitude was of 0.2 V and the frequency range from 10 mHz to 100 kHz.

To precisely confirm this claim, CO was allowed to be adsorbed at open circuit potential for 10 min and then stripped oxidatively in CO-free electrolyte containing 0.5 M Na_2SO_4 (pH ~3.5) at the Pt_1Cu_0, Pt_1Cu_1, Pt_1Cu_2, Pt_1Cu_3, and Pt_1Cu_4 catalysts (Fig. 9a-e, respectively). The Pt_1Cu_0 catalyst (Fig. 9a) showed (in the anodic scan) a zero current (Pt surface was blocked) up to ca. 0.73 V where CO started to desorb [64,65]. The charge (Q_{CO}) consumed in the CO stripping is proportional to the poisoning level of CO_{ads} and the onset potential of CO desorption ($E_{onset/CO}$) assess the minimum energy required for this desorption, which also accounts for the electronic properties of the Pt surface. Fortunately, the data of Fig. 9 agreed with the hypotheses of Fig. 8 in suggesting prevailing the electronic element in the catalytic enhancement of the Pt_1Cu_1 and Pt_1Cu_2 catalysts. This was obvious in the increased negative shift of their $E_{onset/CO}$ (Fig. 9b and c). However, the amount of Cu in the Pt_1Cu_1 catalyst was not sufficient to provide an overall (electronic and geometric) enhancement for CO adsorption. The behavior of the Pt_1Cu_2 catalyst was much better in terms of Q_{CO} and $E_{onset/CO}$. Interestingly, regardless the approximate agreement in their $E_{onset/CO}$, the

Table 3 Summary of the electrochemical data extracted from Fig. 8.

Catalyst	R_s (kΩ)	$R_s + R_{ct}$ (kΩ)	R_{ct} (kΩ)
Pt_1Cu_0	0.28	0.49	0.21
Pt_1Cu_1	0.29	0.43	0.14
Pt_1Cu_2	0.28	0.43	0.15
Pt_1Cu_3	0.28	0.55	0.27
Pt_1Cu_4	0.28	0.71	0.43

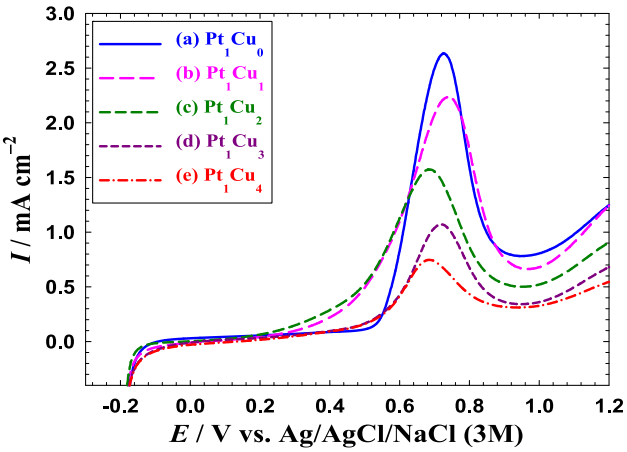

Fig. 9 Oxidative stripping of CO measured in aqueous solution of 0.5 M Na_2SO_4 (pH ~ 3.5) at the (a) Pt_1Cu_0, (b) Pt_1Cu_1, (c) Pt_1Cu_2, (d) Pt_1Cu_3, and (e) Pt_1Cu_4. The potential scan rate = 50 mV s^{-1}. Before measurement, CO was allowed to be chemisorbed from 0.5 M FA.

Table 4 Summary of the electrochemical data extracted from Fig. 9.

Catalyst	Q_{CO} (mC)	$E_{onset/CO}$ (mV)
Pt_1Cu_0	1.47	475
Pt_1Cu_1	1.51	302
Pt_1Cu_2	1.10	251
Pt_1Cu_3	0.59	407
Pt_1Cu_4	0.37	418

Pt_1Cu_3 and Pt_1Cu_4 catalysts retained much lower Q_{CO} than that of the Pt_1Cu_0 catalyst which highlighted the geometrical influence in retarding the adsorption of poisoning CO at the Pt surface. Table 4 summarizes the data obtained from Fig. 9 which confirmed ca. 25, 60 and 75% improvement in the CO tolerance on the Pt surface of the Pt_1Cu_2, Pt_1Cu_3 and Pt_1Cu_4 catalysts, respectively. This confirmed the structural (third body) enhancement for the Pt_1Cu_2, Pt_1Cu_3, and Pt_1Cu_4 catalysts. Besides, Cu could also facilitate the oxidative removal of CO at lower potentials (electronic impact) at the Pt_1Cu_1 and Pt_1Cu_2 catalysts as respectively shown from the −0.17 and −0.22 V shift $E_{onset/CO}$. Lastly, it is important to mention that although the Pt_1Cu_4 catalyst did not show any electronic enhancement, it acquired the highest activity and stability toward FAOR that originated solely from its structural (third body) enhancement effect.

4. Conclusion

A Pt_xCu_y binary catalyst was endorsed for efficient FAOR. The molar ratio of Pt^{4+} and Cu^{2+} ions in the deposition bath influenced, to a high degree, the catalytic performance and the enhancement mechanism toward FAOR. The Pt_1Cu_4 catalyst retained the highest catalytic activity (with up to ca. 6 times increase in the I_p^d/I_p^{ind} index, 4 times increase in the I_p^d/I_p^b index and −336 mV shift in E_{onset}) of FAOR. This associated critical improvement in the catalytic stability that appeared in maintaining the highest current density and lowest current decay during prolonged electrolysis at 0.2 V, comparing to all other inspected catalysts. Based on the EIS and the CO stripping measurements, the catalytic enhancement of the Pt_1Cu_4 catalyst arose principally from a structural (third body) effect.

Declaration of Competing Interest

The authors declare that they have no known competing financial interests or personal relationships that could have appeared to influence the work reported in this paper.

Appendix A. Supplementary data

Supplementary data to this article can be found online at https://doi.org/10.1016/j.jscs.2022.101437.

References

[1] U.S.E.I.A.s., International Energy Outlook, Office of Energy Analysis. U.S. Department of Energy, Washington DC (2019) 20585.
[2] Y.M. Asal, I.M. Al-Akraa, A.M. Mohammad, M.S. El-Deab, A competent simultaneously co-electrodeposited Pt-MnOx nanocatalyst for enhanced formic acid electro-oxidation, J. Taiwan Inst. Chem. Eng. 96 (2019) 169–175.
[3] Z. Li, L. Cai, M. Song, Y. Shen, X. Wang, J. Li, J. Wang, P. Wang, L. Tian, Ternary FeCoNi alloy nanoparticles embedded in N-doped carbon nanotubes for efficient oxygen evolution reaction electrocatalysis, Electrochim. Acta 339 (2020) 135886.
[4] H. Xu, H. Shang, C. Wang, Y. Du, Low-Dimensional Metallic Nanomaterials for Advanced Electrocatalysis, Adv. Funct. Mater. 30 (2020) 2006317.
[5] I.M. Al-Akraa, A.E. Salama, Y.M. Asal, A.M. Mohammad, Boosted performance of NiOx/Pt nanocatalyst for the electro-oxidation of formic acid: A substrate's functionalization with multi-walled carbon nanotubes, Arab J Chem. 14 (2021) 103383.
[6] Y.M. Asal Preparation of Co-electrodeposited Pd-Au nanocatalyst for methanol electro-oxidation Int. J. Electrochem. Sci. Article ID:211133 10.20964/2021.11.30
[7] Z. Li, M. Song, W. Zhu, W. Zhuang, X. Du, L. Tian, MOF-derived hollow heterostructures for advanced electrocatalysis, Coord. Chem. Rev. 439 (2021) 213946.
[8] T. Ma, C. Li, T. Liu, Q. Yuan, Size-controllable synthesis of dendritic Pd nanocrystals as improved electrocatalysts for formic acid fuel cells' application, J. Saudi Chem. Soc. 22 (7) (2018) 846–854.
[9] W. Hong, C. Shang, J. Wang, E. Wang, Bimetallic PdPt nanowire networks with enhanced electrocatalytic activity for ethylene glycol and glycerol oxidation, Energy Environ. Sci. 8 (2015) 2910–2915.
[10] A.S. Abdulhalim, Y.M. Asal, A.M. Mohammad, I.M. Al-Akraa, Ni-Au anodic nano-electrocatalyst for direct glucose fuel cells, Int. J. Electrochem. Sci. 15 (2020) 3274–3282.
[11] H. Xu, H. Shang, C. Wang, Y. Du, Ultrafine Pt-based nanowires for advanced catalysis, Adv. Funct. Mater. 30 (2020) 2000793.
[12] A. Coralli, B.J.M. Sarruf, P.E.V. de Miranda, O. Luigi, S. Specchia, N.Q. Minh, Chapter 2 - Fuel cells, in: P.E.V. de Miranda (Ed.), Science and Engineering of Hydrogen-Based Energy Technologies, Academic Press, 2019, pp. 39–122.
[13] I.M. Al-Akraa, A.M. Mohammad, A spin-coated TiOx/Pt nanolayered anodic catalyst for the direct formic acid fuel cells, Arab J Chem. 13 (2020) 4703–4711.

[14] M.S. El-Deab, G.H. El-Nowihy, A.M. Mohammad, Synergistic enhancement of the electro-oxidation of methanol at tailor-designed nanoparticle-based CoOx/MnOx/Pt ternary catalysts, Electrochim. Acta 165 (2015) 402–409.
[15] G. Şefkat, M.A. Özel, Experimental and numerical study of energy and thermal management system for a hydrogen fuel cell-battery hybrid electric vehicle, Energy 238 (2022) 121794.
[16] I.M. Al-Akraa, B.A. Al-Qodami, M.S. Santosh, A.K. Thottoli, A.M. Mohammad, Tuning the activity and stability of platinum nanoparticles toward the catalysis of the formic acid electrooxidation, Int. J. Electrochem. Sci. 15 (2020) 5597–5608.
[17] U.B. Demirci, Direct liquid-feed fuel cells: Thermodynamic and environmental concerns, J. Power Sources 169 (2) (2007) 239–246.
[18] Z. Teng, M. Li, Z. Li, Z. Liu, G. Fu, Y. Tang, Facile synthesis of channel-rich ultrathin palladium-silver nanosheets for highly efficient formic acid electrooxidation, Mater. Today Energy 19 (2021) 100596.
[19] H. Meng, D. Zeng, F. Xie, Recent development of Pd-based electrocatalysts for proton exchange membrane fuel cells, Catalysts 5 (2015) 1221–1274.
[20] I.M. Al-Akraa, A.M. Mohammad, M.S. El-Deab, B.E. El-Anadouli, On the catalytic activity of palladium nanoparticles-based anodes towards formic acid electro-oxidation: effect of electrodeposition potential, progress in clean, Energy 1 (2015) 559–570.
[21] S. Bong, B. Jang, D. Han, Y. Piao, Effective electrochemical activation of oleate-residue-fouled Pt nanoparticle catalysts for methanol and formic acid oxidation, ACS Omega 4 (2019) 20330–20334.
[22] H.M. An, Z.L. Zhao, L.Y. Zhang, Y. Chen, Y.Y. Chang, C.M. Li, Ir-alloyed ultrathin ternary PdIrCu nanosheet-constructed flower with greatly enhanced catalytic performance toward formic acid electrooxidation, ACS Appl. Mater. Interfaces 10 (2018) 41293–41298.
[23] Y. Wang, X. Jiang, G. Fu, Y. Li, Y. Tang, J.-M. Lee, Y. Tang, Cu_5Pt dodecahedra with low-Pt content: facile synthesis and outstanding formic acid electrooxidation, ACS Appl. Mater. Interfaces 11 (2019) 34869–34877.
[24] S. Maturost, S. Themsirimongkon, S. Saipanya, L. Fang, N. Pongpichayakul, J. Jakmunee, P. Waenkaew, Carbon nanotube-copper oxide-supported palladium anode catalysts for electrocatalytic enhancement in formic acid oxidation, Int. J. Hydrogen Energy (2021) In press.
[25] I.M. Al-Akraa, A.M. Mohammad, M.S. El-Deab, B.E. El-Anadouli, Electrocatalysis by design: Synergistic catalytic enhancement of formic acid electro-oxidation at core–shell Pd/Pt nanocatalysts, Int. J. Hydrogen Energy 40 (2015) 1789–1794.
[26] L. Yang, G. Li, J. Chang, J. Ge, C. Liu, F. Vladimir, G. Wang, Z. Jin, W. Xing, Sea urchin-like Aucore@Pdshell electrocatalysts with high FAOR performance: Coefficient of lattice strain and electrochemical surface area, Appl. Catal. B: Environ. 260 (2020) 118200.
[27] B.D. Adams, R.M. Asmussen, C.K. Ostrom, A. Chen, Synthesis and comparative study of nanoporous palladium-based bimetallic catalysts for formic acid oxidation, J. Phys. Chem. C 118 (51) (2014) 29903–29910.
[28] S. Xu, J. Zhang, J. Wang, L. Lv, Y. Sun, X. Huang, T. Lin, X. Huang, L. Shao, The electrooxidation of formic acid catalyzed by Pd–Ga nanoalloys, Catal. Sci. Technol. 9 (2019) 1255–1259.
[29] Y. Sun, B. Huang, Y. Li, Y. Qin, Z. Fu, M. Sun, L. Wang, S. Guo, Segmented Au/PtCo heterojunction nanowires for efficient formic acid oxidation catalysis, Fundam. Res. 1 (2021) 453–460.
[30] G.A. El-Nagar, A.M. Mohammad, Enhanced electrocatalytic activity and stability of platinum, gold, and nickel oxide nanoparticles-based ternary catalyst for formic acid electro-oxidation, Int. J. Hydrogen Energy 39 (2014) 11955–11962.
[31] I.M. Al-Akraa, Y.M. Asal, S.A. Darwish, A simple and effective way to overcome carbon monoxide poisoning of platinum surfaces in direct formic acid fuel cells, Int. J. Electrochem. Sci. 14 (2019) 8267–8275.
[32] Y.M. Asal, I.M. Al-Akraa, A.M. Mohammad, M.S. El-Deab, Design of efficient bimetallic Pt–Au nanoparticle-based anodes for direct formic acid fuel cells, Int. J. Hydrogen Energy 44 (2019) 3615–3624.
[33] X. Jiang, Y. Xiong, Y. Wang, J. Wang, N. Li, J. Zhou, G. Fu, D. Sun, Y. Tang, Treelike two-level Pd_xAg_y nanocrystals tailored for bifunctional fuel cell electrocatalysis, J. Mater. Chem. A 7 (2019) 5248–5257.
[34] X. Cao, Y. Han, C. Gao, X. Huang, Y. Xu, N. Wang, PtAg nanowires: facile synthesis and their applications as excellent oxygen reduction electrocatalysts for label-free electrochemical immunoassay, J. Mater. Chem. A 1 (2013) 14904–14909.
[35] N. Becknell, Y. Kang, C. Chen, J. Resasco, N. Kornienko, J. Guo, N.M. Markovic, G.A. Somorjai, V.R. Stamenkovic, P. Yang, Atomic structure of Pt_3Ni nanoframe electrocatalysts by in situ X-ray absorption spectroscopy, J. Am. Chem. Soc. 137 (2015) 15817–15824.
[36] S. Maturost, N. Pongpichayakul, P. Waenkaew, N. Promsawan, S. Themsirimongkon, J. Jakmunee, S. Saipanya, Electrocatalytic activity of bimetallic PtPd on cerium oxide-modified carbon nanotube for oxidation of alcohol and formic acid, J. Electroanal. Chem. 895 (2021) 115445.
[37] T. Chen, C. Ge, Y. Zhang, Q. Zhao, F. Hao, N. Bao, Bimetallic platinum–bismuth nanoparticles prepared with silsesquioxane for enhanced electrooxidation of formic acid, Int. J. Hydrogen Energy 40 (2015) 4548–4557.
[38] G.A. El-Nagar, A.M. Mohammad, M.S. El-Deab, B.E. El-Anadouli, Propitious dendritic Cu_2O–Pt nanostructured anodes for direct formic acid fuel cells, ACS Appl. Mater. Interfaces 9 (2017) 19766–19772.
[39] B.A. Al-Qodami, H.H. Alalawy, I.M. Al-Akraa, S.Y. Sayed, N. K. Allam, A.M. Mohammad, Surface engineering of nanotubular ferric oxyhydroxide "goethite" on platinum anodes for durable formic acid fuel cells, Int. J. Hydrogen Energy 47 (2022) 264–275.
[40] O. Sancakoglu, A new approach — in-situ codeposition of composite coatings, in: A.M.A. Mohamed, T.D. Golden (Eds.), Electrodeposition of Composite Materials, InTech, 2016.
[41] T. Binninger, E. Fabbri, R. Kötz, T.J. Schmidt, Determination of the Electrochemically Active Surface Area of Metal-Oxide Supported Platinum Catalyst, J. Electrochem. Soc. 161 (3) (2014) H121–H128.
[42] X. Li, Y. Zhou, Y. Du, J. Xu, W. Wang, Z. Chen, J. Cao, PtCu nanoframes as ultra-high performance electrocatalysts for methanol oxidation, Int. J. Hydrogen Energy 44 (2019) 18050–18057.
[43] Y.i. Yang, Y.-F. Guo, C.e. Fu, R.-H. Zhang, W. Zhan, P. Wang, X. Zhang, Q.i. Wang, X.-W. Zhou, In-situ loading synthesis of graphene supported PtCu nanocube and its high activity and stability for methanol oxidation reaction, J. Colloid Interface Sci. 595 (2021) 107–117.
[44] C. Zhang, Y. Zhang, H. Xiao, J. Zhang, L. Li, L. Wang, Q. Bai, M. Liu, Z. Wang, N. Sui, Superior catalytic performance and CO tolerance of PtCu/graphdiyne electrocatalyst toward methanol oxidation reaction, Colloids Surf. A Physicochem. Eng. Asp. 612 (2021) 125960.
[45] F. Caballero-Briones, J.M. Artés, I. Díez-Pérez, P. Gorostiza, F. Sanz, Direct observation of the valence band edge by in situ ECSTM-ECTS in p-type Cu_2O layers prepared by copper anodization, J. Phys. Chem. C 113 (2009) 1028–1036.
[46] C. Toparli, A. Sarfraz, A. Erbe, A new look at oxide formation at the copper/electrolyte interface by in situ spectroscopies, Phys. Chem. Chem. Phys. 17 (2015) 31670–31679.

[47] L. Luu, N. Tri, H. Cuong, M. Hoang, A. Ha, The role of carriers in properties and performance of Pt-CuO nanocatalysts in low temperature oxidation of CO and p-xylene, Adv. Nat. Sci.: Nanosci. Nanotechnol. 6 (2015) 01501.
[48] W. Duan, A. Li, Y. Chen, K. Zhuo, J. Liu, J. Wang, Ionic liquid-assisted synthesis of reduced graphene oxide–supported hollow spherical PtCu alloy and its enhanced electrocatalytic activity toward methanol oxidation, J. Nanopart. Res. 20 (2018) 287.
[49] A. Liu, Z. Shi, R.G. Reddy, Mechanism study of Cu-Zn alloys electrodeposition in deep eutectic solvents, Ionics 26 (2020) 3161–3172.
[50] T.M. Keller, S.B. Qadri, C.A. Little, Carbon nanotube formation in situ during carbonization in shaped bulk solid cobalt nanoparticle compositions, J. Mater. Chem. 14 (2004) 3063–3070.
[51] H. Kahler, The crystalline structures of sputtered and evaporated metallic films, Phys. Rev. 18 (1921) 210–217.
[52] T. Thirugnanasambandan, M. Alagar, X-ray diffraction studies of copper nanopowder, Arch. Phys. Res. 1 (2010) 112–117.
[53] H.D. Omar, The analysis of copper-iron metallic mixture by means of XRD and XRF, Int. Lett. Chem. Phys. Astron. 64 (2016) 130–134.
[54] I.-K. Suh, H. Ohta, Y. Waseda, High-temperature thermal expansion of six metallic elements measured by dilatation method and X-ray diffraction, J. Mater. Sci. 23 (1988) 757–760.
[55] B. Hu, J. Yuan, J. Zhang, Q. Shu, D. Guan, G. Yang, W. Zhou, Z. Shao, High activity and durability of a Pt–Cu–Co ternary alloy electrocatalyst and its large-scale preparation for practical proton exchange membrane fuel cells, Compos. B Eng. 222 (2021) 109082.
[56] G.A. El-Nagar, A.M. Mohammad, M.S. El-Deab, B.E. El-Anadouli, Electrocatalysis by design: Enhanced electrooxidation of formic acid at platinum nanoparticles–nickel oxide nanoparticles binary catalysts, Electrochim. Acta 94 (2013) 62–71.
[57] L. Lu, L. Shen, Y.i. Shi, T. Chen, G. Jiang, C. Ge, Y. Tang, Y.u. Chen, T. Lu, New insights into enhanced electrocatalytic performance of carbon supported Pd–Cu catalyst for formic acid oxidation, Electrochim. Acta 85 (2012) 187–194.
[58] G.A. El-Nagar, A.M. Mohammad, M.S. El-Deab, B.E. El-Anadouli, Facilitated electro-oxidation of formic acid at nickel oxide nanoparticles modified electrodes, J. Electrochem. Soc. 159 (2012) F249–F254.
[59] A.A. Balandin, The multiplet theory of catalysis, structural factors in catalysis, Russ. Chem. Rev. 31 (1962) 589–614.
[60] E. Yavuz, K. Volkan Özdokur, I. Çakar, S. Koçak, F. Nil Ertaş, Electrochemical preparation, characterization of molybdenum-oxide/platinum binary catalysts and its application to oxygen reduction reaction in weakly acidic medium, Electrochim. Acta 151 (2015) 72–80.
[61] I.M. Al-Akraa, A.M. Mohammad, M.S. El-Deab, B.E. El-Anadouli, Flower-shaped gold nanoparticles: Preparation, characterization, and electrocatalytic application, Arab. J. Chem. 10 (2017) 877–884.
[62] N.A. Pelot, B.J. Thio, W.M. Grill, Modeling current sources for neural stimulation in COMSOL, Front. Comput. Neurosci. 12 (2018).
[63] A.P. Leggiero, S.D. Driess, E.D. Loughran, D.J. McIntyre, R. K. Hailstone, C.D. Cress, I. Puchades, B.J. Landi, Platinum nanometal interconnection of copper–carbon nanotube hybrid electrical conductors, Carbon 168 (2020) 290–301.
[64] A.M. Mohammad, I.M. Al-Akraa, M.S. El-Deab, Superior electrocatalysis of formic acid electro-oxidation on a platinum, gold and manganese oxide nanoparticle-based ternary catalyst, Int. J. Hydrogen Energy 43 (2018) 139–149.
[65] A.M. Mohammad, G.A. El-Nagar, I.M. Al-Akraa, M.S. El-Deab, B.E. El-Anadouli, Towards improving the catalytic activity and stability of platinum-based anodes in direct formic acid fuel cells, Int. J. Hydrogen Energy 40 (2015) 7808–7816.